

Quasiparticle Mass Enhancement and Fermi Surface Shape Modification in Oxide Two-Dimensional Electron Gases

John R. Tolsma,^{1,*} Alessandro Principi,² Reza Asgari,³ Marco Polini,⁴ and Allan H. MacDonald¹

¹*Department of Physics, The University of Texas at Austin, Austin Texas 78712, USA*

²*Radboud University of Nijmegen, Institute for Molecules and Materials, Heijendaalseweg 135, 6525 AJ Nijmegen, The Netherlands*

³*School of Physics, Institute for Research in Fundamental Sciences (IPM), Tehran 19395-5531, Iran*

⁴*Istituto Italiano di Tecnologia, Graphene Labs, Via Morego 30, I-16163 Genova, Italy*

(Dated: October 20, 2015)

We propose a model intended to qualitatively capture the electron-electron interaction physics of two-dimensional electron gases formed near transition-metal oxide heterojunctions containing t_{2g} electrons with a density much smaller than one electron per metal atom. Two-dimensional electron systems of this type can be described perturbatively using a GW approximation which predicts that Coulomb interactions enhance quasiparticle effective masses more strongly than in simple two-dimensional electron gases, and that they reshape the Fermi surface, reducing its anisotropy.

PACS numbers: 71.10.-w, 71.18.+y, 73.21.-b

I. INTRODUCTION

Transition-metal oxides in three dimensions display an amazing variety of novel phenomena, from high-temperature superconductivity and colossal magnetoresistance to orbital ordering and metal-insulator phase transitions. Because the metal d -bands present near their Fermi levels tend to be narrow and sensitive to oxygen coordination, both electron-electron and electron-lattice interactions are often strong. When the number of d -electrons per transition metal site is close to an integer, the most important electron-electron interactions occur on the atomic length scale and can be captured by Hubbard-type model interactions¹. In d -band systems it is also often important to distinguish the manner in which d -orbitals form bonds with neighboring oxygen ions². These two features provide a framework for analyzing many strongly interacting bulk transition-metal oxide crystals.

It has recently³⁻⁷ become possible to realize two-dimensional quantum wells based on heterojunctions between transition-metal oxides, and while the nature of d -electron bonding remains important, Hubbard-like correlations are often not. To date the most common quantum well material is SrTiO₃ and the number of d -electrons per metal in the quantum wells is typically, although not always^{8,9}, much less than one. Oxide two-dimensional electron systems have application potential because, as in the case of covalent semiconductors, large relative changes in the quantum well carrier density can be achieved by electrical means. The conduction bands of these systems are formed from t_{2g} electrons that are weakly π -bonded to neighboring oxygens, and consequently form rather narrow and anisotropic bands. When the electron density per metal atom is much smaller than one, the Fermi surface occupies a small fraction of the Brillouin zone and the probability of two electrons simultaneously occupying the same transition-metal site is

small. In this limit, including only the Hubbard part of the full electron-electron interaction misses the most important Coulomb interactions. Because of its long range the typical Coulomb interaction energy of an individual electron drops to zero only as two-dimensional density $n^{1/2}$, in contrast to the $\propto n$ behavior of the Hubbard model. Indeed, the full long-range of the Coulomb potential must be recognized in any theory of electron-electron interaction effects in semimetal or doped semiconductor small-Fermi-surface systems. The long-range Coulomb potential plays a critical role in the theory of plasmon oscillations¹⁰⁻¹³, quasiparticle effective mass¹⁴⁻¹⁶, angle-resolved photoemission spectra^{17,18}, and many other observables^{19,20}.

In this Article we introduce a generic model for two-dimensional t_{2g} electron gases which captures both the anisotropic character of the d -orbitals forming the low-energy conduction bands, and the importance of long-range Coulomb interactions when the number of conduction electrons per transition-metal site is much less than one. The t_{2g} two-dimensional electron gas model we introduce is informed by recent self-consistent Hartree/tight-binding^{21,22} and *ab initio* calculations²³⁻²⁵ for SrTiO₃ quantum wells. As a first application of this model, we calculate some observable quasiparticle properties of electrons in the anisotropic bands. Our Article is organized as follows. In Section II we describe the t_{2g} two-dimensional electron gas model and discuss the limits of its validity as a model of SrTiO₃ quantum wells. In Section III we describe the G_0W approximation for the quasiparticle self-energy and present explicit expressions for its *line-residue* decomposition²⁶. We use these expressions to calculate the renormalized Fermi surface shape in Section IV and the quasiparticle mass enhancement in Section V. Finally, in Section VI we present our conclusions.

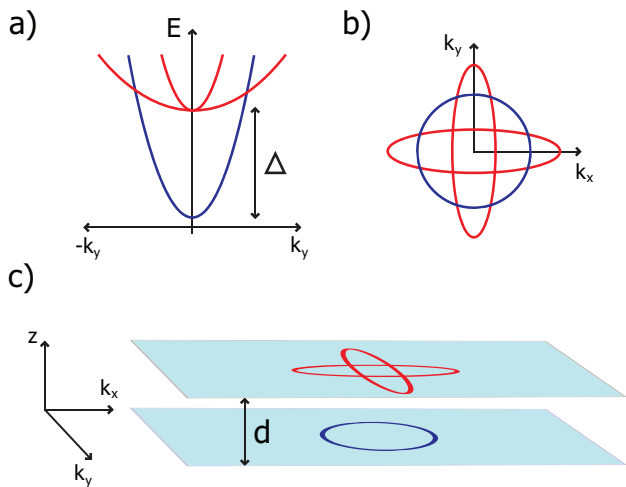


FIG. 1: (Color online) A schematic summary of the t_{2g} two-dimensional electron gas model. In a) the energy offset Δ between the anisotropic xz and yz (red) band edge and the isotropic xy (blue) band edge is emphasized. In b) the anisotropy of the elliptical xz and yz Fermi surfaces (red) is contrasted with the xy band's circular Fermi surface (blue). The lower panel highlights the difference in \hat{z} -direction confinement between the xz and yz bands and the xy band, which can be crudely characterized by a separation distance d .

II. THE t_{2g} TWO-DIMENSIONAL ELECTRON GAS MODEL

The many-body effects of long-range Coulomb interactions in covalent semiconductors are often studied using continuum electron gas models^{19,20}. In order to apply a similar approach to the two-dimensional electron gas residing at heterojunctions between SrTiO₃ and a barrier material, it is necessary to account for some key differences. These are captured by the t_{2g} two-dimensional electron gas (t_{2g} 2DEG) model which we now detail. The three distinct characteristics of t_{2g} 2DEGs are band-mass anisotropy, a energy offset between the band edges of subbands with different masses along the confinement direction, and a band-dependence in the distance between two-dimensional subband density maxima and the heterojunction or surface. Figure 1 illustrates these three features. The model parameters we choose for the illustrative calculations we describe later in this Article are informed by recent tight-binding^{21,22} and *ab initio* calculations²³⁻²⁵ for SrTiO₃ 2DEGs. The t_{2g} 2DEG model can be adapted to other materials by adjusting the model parameter choices.

The anisotropic nearest-neighbor effective metal-to-metal hopping amplitudes of t_{2g} orbitals are ultimately responsible for many of the distinct characteristics of the t_{2g} 2DEG. In three-dimensional SrTiO₃, crystal-field splitting breaks the 5-fold degeneracy amongst the Ti d-orbitals. The xy , yz , and xz orbitals (*i.e.* the t_{2g} orbitals) are lower in energy because they bond less strongly with neighboring oxygens and form the bulk con-

duction bands in n-type semiconducting SrTiO₃. Electronic hopping between t_{2g} d-orbitals on different Ti sites proceeds in a two-step process via the octahedrally coordinated oxygen p-orbitals surrounding each Ti atom^{2,21,23,27}. Orbital symmetry dictates that each t_{2g} electron hops mainly between states with the same orbital character, with a large hopping amplitude t in two directions, and a smaller hopping amplitude t' in the third. This leads to separate t_{2g} bands with xy , yz , and xz d-orbital character that have a light mass m_L in two directions, and a heavy mass m_H in the third direction. The weak hopping directions for xy , xz , and yz are \hat{z} , \hat{y} , and \hat{x} , respectively. The heavy masses are therefore in perpendicular directions for the three orbital characters. In the presence of a \hat{z} -direction confining potential strong enough to produce an effectively two-dimensional system, the xy band has two light masses in-plane, while the xz and yz bands have one heavy and one light mass in-plane (see Fig. 1). According to recent tight-binding fits²¹ to Shubnikov-de Haas measurements²⁸ of bulk n-type SrTiO₃, $m_H = \hbar^2/(2t'a^2)$ and $m_L = \hbar^2/(2ta^2)$ where $t = 236$ meV, $t' = 35$ meV, and the lattice constant $a = 3.9$ Å. This implies that

$$\frac{m_H}{m} = \frac{Ry}{t'} \left(\frac{a_B}{a} \right)^2 \sim 7 \quad (1)$$

and

$$\frac{m_L}{m} = \frac{Ry}{t} \left(\frac{a_B}{a} \right)^2 \sim 1, \quad (2)$$

where m is the bare electron mass in vacuum, $a_B = \hbar^2/(me^2) = 0.529$ Å is the Bohr radius, and $Ry = \hbar^2/(2ma_B^2) = 13.6$ eV is the Rydberg energy. These values for the heavy and light mass are in good agreement with angle-resolve photoemission spectrum measurements on bulk SrTiO₃²⁹.

As a result of these relatively large effective band-mass values and the non-linear and non-local dielectric screening properties of bulk SrTiO₃, subband splitting is relatively small and several subbands of xy , yz , and xz type are expected to be occupied even at moderate electron densities^{21,22,24}. However, since even in this case $\gtrsim 75\%$ of the electron density is contained in the lowest xy , yz and xz subband²¹, in the t_{2g} 2DEG model we address the case in which only one subband of each orbital type is occupied. This model is sufficiently realistic to account for the most interesting peculiarities of this type of 2DEG and can be generalized if there is interest in describing the properties of particular 2DEG systems which have more occupied subbands. Figure 1 illustrates the anisotropy of the xz and yz bands in the three-band t_{2g} 2DEG model.

In addition to the band-mass anisotropy, two other important characteristics of the t_{2g} electron gas model follow from the anisotropic hopping amplitudes of the t_{2g} d-orbitals. First, because xz and yz electrons have a much larger hopping amplitude in the \hat{z} -direction (which we take to be the confinement direction) than the xy electrons whose heavy mass is in the \hat{z} -direction, the former

are less easily confined to the same surface or to an interface of a heterojunction system^{21,25}. This separation introduces an orbital dependence to the electron-electron interactions which we capture by introducing an effective distance d between the xy and the xz and yz bands. Realistic values of d in SrTiO₃ can be estimated from previously published studies of the layer dependent t_{2g} density distribution as a function of confinement field^{21,22}. The effective separation decreases for increasing interfacial confinement field and total t_{2g} density and lies in the range $d = 2a - 10a$ for t_{2g} electron densities between $2 \times 10^{13} \text{ cm}^{-2} - 3 \times 10^{14} \text{ cm}^{-2}$. Second, mass differences in the confinement direction leads to a finite energy offset Δ between the conduction band edges of the xy and the xz - yz bands, see Fig. 1a). The band offset increases for larger confinement field (total t_{2g} density) and in SrTiO₃ theory has proposed that $\Delta = 10 - 200 \text{ meV}$ ²¹, in reasonable agreement with the range of values found in recent experiments³⁰⁻³².

Motivated by these three distinct characteristics of t_{2g} 2DEGs and recognizing that it is necessary to account for the long-range Coulomb interaction, we propose the following Hamiltonian for the t_{2g} 2DEG:

$$\begin{aligned} \mathcal{H}_{t_{2g}} = & \sum_{\mathbf{k}\alpha} \varepsilon_{\alpha}(\mathbf{k}) \hat{c}_{\mathbf{k}\alpha}^{\dagger} \hat{c}_{\mathbf{k}\alpha} \\ & + \frac{1}{2A} \sum_{\mathbf{q} \neq 0} \sum_{\substack{\mathbf{k}\mathbf{k}' \\ \alpha\alpha'}} V_{\alpha\alpha'}(\mathbf{q}) c_{\mathbf{k}+\mathbf{q}\alpha}^{\dagger} c_{\mathbf{k}'-\mathbf{q}\alpha'}^{\dagger} c_{\mathbf{k}'\alpha'} c_{\mathbf{k}\alpha}, \end{aligned} \quad (3)$$

where α represents both spin and band-orbital quantum numbers, A is the 2D sample area, and the Fourier transform of the 2D Coulomb interaction is

$$V_{\alpha\alpha'}(\mathbf{q}) = \frac{2\pi e^2}{\kappa q} e^{-qd_{\alpha\alpha'}} \equiv v_q e^{-qd_{\alpha\alpha'}}, \quad (4)$$

with $q = |\mathbf{q}|$. Here, κ is an effective dielectric constant and $d_{\alpha\alpha'}$ gives the effective confinement-direction separation distance between an electron with band index α and an electron with band index α' . For the typical electron-electron interaction transition energies in t_{2g} electron gases the relevant dielectric constant does not include soft-phonon contributions³³, but depends on the dielectric environment on both sides of the relevant heterojunction or surface. The t_{2g} band energies near the band minimum are

$$\varepsilon_{\alpha}(\mathbf{k}) = \begin{cases} \frac{\hbar^2 \mathbf{k}^2}{2m_L} & \text{for } \alpha = xy, \sigma \\ \frac{\hbar^2 k_x^2}{2m_L} + \frac{\hbar^2 k_y^2}{2m_H} + \Delta & \text{for } \alpha = xz, \sigma \\ \frac{\hbar^2 k_x^2}{2m_H} + \frac{\hbar^2 k_y^2}{2m_L} + \Delta & \text{for } \alpha = yz, \sigma \end{cases}, \quad (5)$$

where m_H and m_L have been introduced earlier in Eqs. (1) and (2), respectively.

The applicability of the proposed t_{2g} 2DEG model (3) to describe SrTiO₃-based 2DEGs depends on the total

electron density. The continuum model for the band structure is valid only if the number of conduction band electrons per Ti site is much smaller than one. Its applicability therefore depends not-only on the carrier density per cross-sectional area, but also on quantum well thickness. On the other hand, we have neglected spin-orbit coupling terms in the band Hamiltonian, which play an essential role at small carrier densities. The t_{2g} 2DEG model is applicable when the density is large enough that spin-orbit coupling, which acts to mix the orbital character of the conduction bands²¹, can be neglected, *i.e.* when the strength of spin-orbit coupling (*e.g.* $\sim 17 \text{ meV}$ in Ref. 28) is small compared to the Fermi energy.

III. THE QUASIPARTICLE SELF-ENERGY IN G_0W -RPA

Coulomb interactions in Fermi liquids, whether doped semiconductors or weakly correlated metals, give rise to two types of elementary excitations^{19,20}: neutral collective excitations and charged quasiparticles. The latter, with which we are concerned in this Article, are excitations with the same quantum numbers as non-interacting independent-particle electronic states. Their energies are shifted from the non-interacting values and their lifetimes are finite, in both cases because of electron-electron interactions.

A self-consistent equation for the quasiparticle excitation energy, *i.e.* the quasiparticle energy measured from the chemical potential, is obtained from the Dyson equation by locating the energies at which the spectral weight of the one-particle retarded Green's function²⁰ is peaked:

$$\mathcal{E}_{\alpha}(\mathbf{k}) = \xi_{\alpha}(\mathbf{k}) + \text{Re} \bar{\Sigma}_{\alpha}(\mathbf{k}, \omega)|_{\omega=\mathcal{E}_{\alpha}(\mathbf{k})/\hbar}, \quad (6)$$

where $\xi_{\alpha}(\mathbf{k}) = \varepsilon_{\alpha}(\mathbf{k}) - \varepsilon_{\alpha}(\mathbf{k}_{F\alpha})$ is the band energy measured relative to the Fermi energy, and in the self-energy $\bar{\Sigma}_{\alpha}(\mathbf{k}, \omega) = \Sigma_{\alpha}(\mathbf{k}, \omega) - \Sigma_{\alpha}(\mathbf{k}_{F\alpha}, 0)$ we subtract the term $\Sigma_{\alpha}(\mathbf{k}_{F\alpha}, 0)$ to account for the interaction correction to the chemical potential μ given by

$$\mu = \varepsilon_{\alpha}(\mathbf{k}_{F\alpha}) + \Sigma_{\alpha}(\mathbf{k}_{F\alpha}, 0). \quad (7)$$

The real part of the self-energy in Eq. (6) yields the many-body contribution to the energy of the quasiparticle state. The quasiparticle energy can be measured by taking angle-resolved photoemission spectra^{17,18}, and more indirectly by performing magneto-transport measurements³⁴⁻³⁶.

The G_0W approach, which we apply below, provides a successful^{15,17,26,37-39} approximation for the quasiparticle self-energy in electronic systems in which long-range Coulomb interactions play an essential role. In the G_0W approximation, we employ the random-phase approximation (RPA) for the screened electron-electron interaction. The screened interaction \mathbf{W} (which is a 3×3 matrix in the band indices α, α') is most simply derived by the following algebraic approach²⁰. A generalized Dyson equation

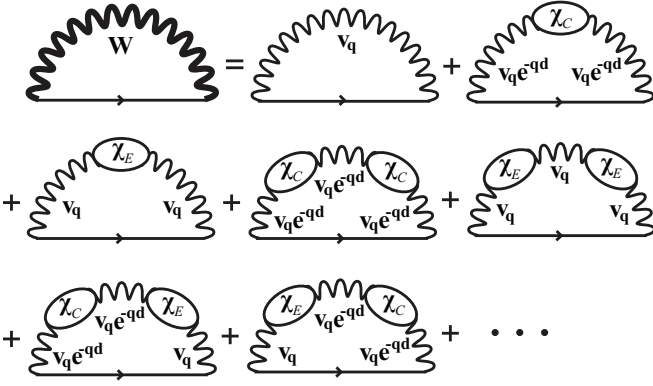


FIG. 2: Feynman diagrams representing the G_0W -RPA approximation for the self-energy of a quasiparticle in one of the elliptical bands of the t_{2g} 2DEG. In RPA the bare (*i.e.* unscreened) Coulomb interaction is dressed (*i.e.* screened) by a infinite series of bubble diagrams representing the density fluctuations of each component (*e.g.* each band) of the system. When applied to the three-band t_{2g} 2DEG, each bubble represents a density fluctuation in either the circular xy band, $\chi_C \equiv \chi_{xy}^{(0)}$, or the elliptical yz and xz bands, $\chi_E \equiv \chi_{yz}^{(0)} + \chi_{xz}^{(0)}$. The circular xy band and the elliptical xz and yz bands have different \hat{z} -direction confinement, which we have crudely accounted for with the separation distance d . As a result, thin wavy lines representing the bare Coulomb interaction are equal to either v_q or $v_q e^{-qd}$ depending on whether the density fluctuations attached to each thin wavy line's endpoints are in the same layer or different layers, respectively. Directed lines represent the non-interaction Green's function of the elliptical-band quasiparticle in question, as in Eq. (16) with $\alpha = yz$ or xz . The thick wavy line represents the fully screened RPA interaction given by Eq. (13).

relates \mathbf{W} to the density-response matrix χ ,

$$\mathbf{W} = \mathbf{V} + \mathbf{V} \cdot \chi \cdot \mathbf{V}, \quad (8)$$

where the matrix of unscreened Coulomb interactions is given by

$$\mathbf{V}(q) \equiv \begin{pmatrix} v_q & v_q e^{-qd} & v_q e^{-qd} \\ v_q e^{-qd} & v_q & v_q \\ v_q e^{-qd} & v_q & v_q \end{pmatrix}. \quad (9)$$

The first, second, and third rows (columns) of each matrix in Eq. (8) correspond to the xy , yz , and xz bands, respectively. In RPA the density-response matrix is related to the diagonal matrix of non-interacting density-response functions $\chi^{(0)}(\mathbf{q}, \omega) \equiv \text{diag}(\chi_{xy}^{(0)}(\mathbf{q}, \omega), \chi_{yz}^{(0)}(\mathbf{q}, \omega), \chi_{xz}^{(0)}(\mathbf{q}, \omega))$ via

$$[\chi(\mathbf{q}, \omega)]^{-1} = [\chi^{(0)}(\mathbf{q}, \omega)]^{-1} - \mathbf{V}(q). \quad (10)$$

Analytic expressions for $\text{Re} \chi_{xy}^{(0)}(\mathbf{q}, \omega)$ and $\text{Im} \chi_{xy}^{(0)}(\mathbf{q}, \omega)$ can be found, for example, in Ref. 20. Expressions for the elliptical-band functions $\chi_{xz}^{(0)}(\mathbf{q}, \omega)$ [$\chi_{yz}^{(0)}(\mathbf{q}, \omega)$] can be easily found by applying the rescaling $k_x \rightarrow$

$k_x \sqrt{m_L/m_{\text{DOS}}}$ and $k_y \rightarrow k_y \sqrt{m_H/m_{\text{DOS}}}$ [$k_x \rightarrow k_x \sqrt{m_H/m_{\text{DOS}}}$ and $k_y \rightarrow k_y \sqrt{m_L/m_{\text{DOS}}}$] in Eq. (5), where $m_{\text{DOS}} = \sqrt{m_L m_H}$ is the density-of-states mass. Since this rescaling maps the elliptical band onto a circular band, the elliptical band density-response functions $\chi_{xz}^{(0)}(\mathbf{q}, \omega)$ and $\chi_{yz}^{(0)}(\mathbf{q}, \omega)$ can be written in terms of $\chi_{xy}^{(0)}(\mathbf{q}, \omega)$:

$$\chi_{xz}^{(0)}(\mathbf{q}, \omega) = \chi_{xy}^{(0)}(q', \omega; m_{\text{DOS}}) \Big|_{q' \rightarrow \sqrt{q_x^2 \zeta^{1/2} + q_y^2 \zeta^{-1/2}}} \quad (11)$$

and

$$\chi_{yz}^{(0)}(\mathbf{q}, \omega) = \chi_{xy}^{(0)}(q', \omega; m_{\text{DOS}}) \Big|_{q' \rightarrow \sqrt{q_x^2 \zeta^{-1/2} + q_y^2 \zeta^{1/2}}} \quad (12)$$

where we have defined $\zeta = m_H/m_L$. Eqs. (8)-(12) can be combined to yield analytic expressions for each element of \mathbf{W} .

Later we will specifically be interested in the screened interaction between two electrons in the anisotropic xz or yz bands while in the presence of a circular xy -band Fermi sea. This particular interaction corresponds to the matrix element $\mathbf{W}_{xz, xz}$ (or equally $\mathbf{W}_{yz, yz}$) which we write as

$$W_{xz}(\mathbf{q}, \omega) \equiv \mathbf{W}_{xz, xz} = \frac{v_q + (e^{-2qd} - 1)v_q^2 \chi_{xy}^{(0)}(\mathbf{q}, \omega)}{\varepsilon(\mathbf{q}, \omega)}, \quad (13)$$

where the RPA dielectric function is given by

$$\varepsilon(\mathbf{q}, \omega) = [1 - v_q \chi_{xy}^{(0)}][1 - v_q (\chi_{xz}^{(0)} + \chi_{yz}^{(0)})] - v_q^2 e^{-2qd} \chi_{xy}^{(0)} (\chi_{xz}^{(0)} + \chi_{yz}^{(0)}), \quad (14)$$

and for brevity we have suppressed the (\mathbf{q}, ω) dependence of the three non-interacting density-response functions appearing in Eq. (14).

In Figure 2 we present the Feynman diagrams which contribute to the G_0W -RPA self-energy of a quasiparticle in one of the elliptical bands of the t_{2g} 2DEG. Summing this infinite series of bubble diagrams (with all of the directed lines representing the non-interacting Green's functions omitted) offers a second route to deriving the RPA interaction $W_{xz}(\mathbf{q}, \omega)$. From Figure 2 we see that density fluctuations in both the circular xy band and the elliptical yz and xz bands contribute to screening, and that density fluctuations in bands with different (the same) \hat{z} -direction confinement, interact with each other via $v_q e^{-qd}$ (v_q). When the Green's functions are included in Figure 2, the series sums to the full G_0W -RPA self-energy. The diagrammatic representation emphasizes that G_0W can be viewed⁴⁰ as an expansion of the self-energy to lowest order in the *screened* electron-electron interaction $W_{xz}(\mathbf{q}, \omega)$.

The finite-temperature⁴¹ G_0W -RPA self-energy of a quasiparticle in band α is given by

$$\Sigma_\alpha(\mathbf{k}, i\omega_n) = -\frac{1}{\beta \hbar A} \sum_{\mathbf{q}, i\Omega_m} W_\alpha(\mathbf{q}, i\Omega_m) \times G_\alpha^{(0)}(\mathbf{k} - \mathbf{q}, i\omega_n - i\Omega_m), \quad (15)$$

where $\beta = (k_B T)^{-1}$ and the fermionic ω_n and bosonic Ω_m Matsubara frequencies are given by $\omega_n = (2n + 1)\pi/\hbar\beta$ and $\Omega_m = 2m\pi/\hbar\beta$, respectively. The non-interacting Green's function is given by

$$G_\alpha^{(0)}(\mathbf{k}, i\omega_n) = \frac{1}{i\omega_n - \xi_\alpha(\mathbf{k})/\hbar}. \quad (16)$$

The physical properties of the interacting system depend on the *retarded* self-energy, which can be obtained from Eq. (15) via analytic continuation, $i\omega_n \rightarrow \omega + i\eta$, only *after* carrying out the Matsubara frequency summation over Ω_m . The so-called line-residue decomposition²⁶ proceeds in the reverse order. By carrying out the analytic continuation of Eq. (15) *before* the frequency summation we obtain the (purely real) *line* contribution to the retarded self-energy

$$\begin{aligned} \Sigma_\alpha^{\text{line}}(\mathbf{k}, \omega) &= -\frac{1}{(2\pi)^3} \int_{-\infty}^{\infty} d\Omega \int d^2\mathbf{q} W_\alpha(\mathbf{q}, i\Omega) \\ &\times G_\alpha^{(0)}(\mathbf{k} - \mathbf{q}, \omega - i\Omega). \end{aligned} \quad (17)$$

The *residue* contribution corrects for performing the analytic continuation before evaluating the frequency sum, and is given by

$$\begin{aligned} \Sigma_\alpha^{\text{res}}(\mathbf{k}, \omega) &= -\frac{1}{(2\pi)^2} \int d^2\mathbf{q} W_\alpha(\mathbf{q}, \omega - \xi_\alpha(\mathbf{k} - \mathbf{q})/\hbar) \\ &\times [\Theta\{-\xi_\alpha(\mathbf{k} - \mathbf{q})\} - \Theta\{\hbar\omega - \xi_\alpha(\mathbf{k} - \mathbf{q})\}], \end{aligned} \quad (18)$$

where $\Theta\{x\}$ is the Heaviside step function. In the next two sections we calculate two important properties of t_{2g} 2DEG quasiparticles based on this formulation of the G_0W -RPA retarded self-energy.

IV. FERMI SURFACE SHAPE MODIFICATION (FSSM)

Consider an ordinary single-band isotropic 2DEG²⁰. When interactions are adiabatically turned on, all quasiparticles on the non-interacting Fermi surface have infinite lifetime and experience identical energy shifts given by Eq. (6) and equal to the interaction contribution to the chemical potential. Because of rotational invariance, the self-energy contribution is a function of the magnitude of \mathbf{k} only. All isoenergy surfaces, including the Fermi surface, continue to be circular in the interacting system. Furthermore, Luttinger's theorem⁴² constrains the Fermi surface area of interacting quasiparticles to equal the Fermi surface area of non-interacting electrons, leading to the conclusion that interactions do not yield a Fermi surface shape modification (FSSM). This simplification is artificial however, since interacting electron systems in solids are never perfectly isotropic. In the presence of anisotropy, the self-energy contribution to the quasiparticle energy spectrum is dependent on the orientation of

\mathbf{k} , and the Fermi surface shape can therefore be renormalized by interactions.

We expect this phenomena to be relevant for the anisotropic xz and yz bands of the t_{2g} electron gas. Each band has an elliptical non-interacting Fermi surface. In the following calculations we assume that the renormalized Fermi surface is sufficiently close in shape to an ellipse, that it can still be characterized by two wavevectors, k_{Fx}^* and k_{Fy}^* , whose values are renormalized by interactions from their non-interacting values k_{Fx} and k_{Fy} . Below we explicitly discuss FSSM for the xz band, which has its semimajor axis in the \hat{y} -direction and semiminor axis in the \hat{x} -direction. Results for the yz band can be found by interchanging k_{Fx}^* and k_{Fy}^* .

Our main finding is that Fermi surface anisotropy is reduced by interactions (see Figs. 3 and 4). This result can be understood qualitatively at the Hartree-Fock level. The exchange (X) self-energy of the xz -band is given by

$$\Sigma_{xz}^X(\mathbf{k}) = -\frac{1}{(2\pi)^2} \int d^2\mathbf{q} \frac{2\pi e^2}{\kappa|\mathbf{k} - \mathbf{q}|} \Theta\{\varepsilon_{Fxx} - \varepsilon_{xz}(\mathbf{q})\}, \quad (19)$$

where ε_{Fxx} is the Fermi energy. Eq. (19) can be easily obtained from Eq. (15) by replacing the dynamically-screened interaction $W_{xz}(\mathbf{q}, i\Omega_m)$ with the bare Coulomb interaction v_q . From Eq. (19) we see that a quasiparticle with quantum number \mathbf{k} will have a self-energy correction that is larger in magnitude when there are more occupied states nearby in momentum space; because of the Coulomb interaction factor, the integrand is large for \mathbf{q} near \mathbf{k} , but only if the state \mathbf{q} is occupied. Since the xz band's non-interacting Fermi surface is elliptical, with its semimajor axis parallel to the \hat{y} -axis, an electron at the Fermi surface in the \hat{y} -direction will have fewer occupied states in its neighborhood than an electron at the Fermi surface in the \hat{x} -direction. It follows that

$$\Sigma_{xz}^X(k_{Fx}) < \Sigma_{xz}^X(k_{Fy}), \quad (20)$$

where we note that the exchange self-energy is always negative. Since all states \mathbf{k} sitting on the Fermi surface must, by definition, have the same quasiparticle energy, the Fermi surface will change shape when interactions are taken into account and the degree of Fermi surface anisotropy will be reduced. Below we report numerical calculations which include beyond Hartree-Fock contributions to the quasiparticle self-energy that confirm this expectation.

A. Linearized self-energy estimate of FSSM

We begin with a numerical approach valid for weak interactions that is rather simple to implement. In Section IV C we solve the problem self-consistently. We will find the two methods give nearly identical results.

When the change in Fermi surface is small relative to its original dimensions, we are well justified in expanding

Eq. (7) to linear-order in $\delta\mathbf{k}_F \equiv \mathbf{k}_F^* - \mathbf{k}_F$. In the limit $\delta k_{Fx}/k_{Fx} \ll 1$ we have

$$\begin{aligned} \mu &= \varepsilon_{xz}(k_{Fx}) + \Sigma_{xz}(k_{Fx}, 0) \\ &+ \delta k_{Fx} \partial_{k_x} [\varepsilon_{xz}(\mathbf{k}) + \Sigma_{xz}(\mathbf{k}, 0)]_{\mathbf{k}=k_{Fx}}. \end{aligned} \quad (21)$$

Similarly for $\delta k_{Fy}/k_{Fy} \ll 1$ we have

$$\begin{aligned} \mu &= \varepsilon_{xz}(k_{Fy}) + \Sigma_{xz}(k_{Fy}, 0) \\ &+ \delta k_{Fy} \partial_{k_y} [\varepsilon_{xz}(\mathbf{k}) + \Sigma_{xz}(\mathbf{k}, 0)]_{\mathbf{k}=k_{Fy}}. \end{aligned} \quad (22)$$

For fixed total elliptical band density

$$k_{Fy} \delta k_{Fx} + k_{Fx} \delta k_{Fy} = 0. \quad (23)$$

The three previous equations can be solved for μ , δk_{Fx} , and δk_{Fy} given self-energy values and wavevector derivatives on the non-interacting Fermi surface. In the top and bottom panel of Fig. 3 we plot k_{Fx}^*/k_{Fx} and k_{Fy}^*/k_{Fy} versus an effective interaction strength parameter r_s defined following the convention commonly used in the single-band 2DEG literature²⁰:

$$n_{xz} = \frac{1}{\pi(a_B^* r_s)^2} \quad (24)$$

where $a_B^* = \kappa a_B / m_{\text{DOS}}$ defines the effective (*i.e.* material) Bohr radius, a_B is the atomic Bohr radius, and $m_{\text{DOS}} = \sqrt{m_H m_L}$ has been introduced earlier. As expected, we find that interactions tend to reduce the anisotropy of the elliptical bands in the t_{2g} 2DEG. For comparison, we also plot in Fig. 3 renormalized Fermi wavevectors calculated for a single-band anisotropic 2DEG with energy dispersion given by

$$\varepsilon(\mathbf{k}) = \frac{\hbar^2 k_x^2}{2m_L} + \frac{\hbar^2 k_y^2}{2m_H} \quad (25)$$

and density $n = n_{xz}$.

When r_s is small, the amount of FSSM is similar in both the xz band of the t_{2g} 2DEG and in the single-band anisotropic 2DEG. This occurs for two reasons. First, $\partial_{k_x} \varepsilon_{xz}(\mathbf{k})|_{\mathbf{k}=k_{Fx}}$ and $\partial_{k_y} \varepsilon_{xz}(\mathbf{k})|_{\mathbf{k}=k_{Fy}}$ are dominant over $\partial_{k_x} \Sigma_{xz}(\mathbf{k}, 0)|_{\mathbf{k}=k_{Fx}}$ and $\partial_{k_y} \Sigma_{xz}(\mathbf{k}, 0)|_{\mathbf{k}=k_{Fy}}$, respectively, in Eq. (21) and Eq. (22) when $r_s \ll 1$. And second, because the leading-order contribution to the self-energy when $r_s \ll 1$ is the exchange self-energy of Eq. (19), which is equal for both the xz band of the t_{2g} 2DEG and the single-band anisotropic 2DEG. The small r_s limit allows for simple explanation because both systems are weakly interacting and well described at leading-order by Hartree-Fock.

The situation is more interesting at large values of r_s where correlation effects are important. Specifically, Figure 3 suggests that while FSSM in the single-band 2DEG saturates at large r_s , FSSM in the anisotropic bands of the t_{2g} 2DEG increases with increasing r_s . As we discuss in detail in the next section, the difference in FSSM occurring in t_{2g} system and in the ordinary 2DEG depends sensitively on the influence of the additional screening due to the presence of several occupied bands.

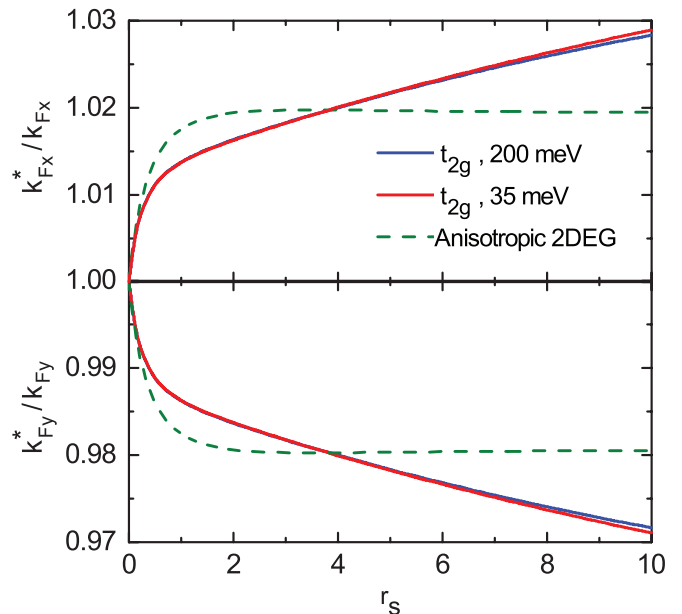


FIG. 3: (Color online) Fractional change in the xz band's Fermi wavevectors, k_{Fx}^*/k_{Fx} (top) and k_{Fy}^*/k_{Fy} (bottom) as a function of interaction strength parameter r_s . The red curve is for band offset $\Delta = 35$ meV and layer separation $d = 10a$ where $a = 3.9$ Å is the SrTiO₃ lattice constant. The blue curve is for band offset $\Delta = 200$ meV and layer separation $d = 2a$. The dashed green curve is for a single-band anisotropic 2DEG whose \hat{x} -direction and \hat{y} -direction non-interacting masses are the same as those of the xz band in the t_{2g} 2DEG model. For this curve r_s is defined from the total density in the single anisotropic band.

B. FSSM at low electron density

Given the G_0W -RPA description of quasiparticles, the principle difference between the anisotropic 2DEG and the xz band of the t_{2g} 2DEG, is that the latter also has electrons occupying the yz and xy bands. To understand how these other occupied conduction bands produce additional screening, and how this screening then qualitatively changes FSSM when density is low, in this section we derive analytic expressions for the self-energy and the wavevector derivative of the self-energy evaluated on the Fermi surface, to leading-order in the small-parameter $1/r_s$. These expressions reveal the basic physical mechanisms which govern FSSM at large r_s within G_0W -RPA theory.

Many of the formulas in this section are written out explicitly for the xz band of the t_{2g} 2DEG, however, analogous expressions for the single-band anisotropic 2DEG can be found by replacing the self-energy of the xz band with the self-energy of the single-band 2DEG. In our numerical calculations, this is carried out simply by setting to zero the density in the xy and yz bands.

We begin by approximating Eq. (21) and Eq. (22) as

$$\frac{\delta k_{Fx}}{k_{Fx}} = \frac{1}{2} \frac{\Sigma_{xz}(k_{Fy}, 0) - \Sigma_{xz}(k_{Fx}, 0)}{k_F \partial_k \Sigma_{xz}(k, 0)|_{k=k_F}} \quad (26)$$

and

$$\frac{\delta k_{Fy}}{k_{Fy}} = \frac{1}{2} \frac{\Sigma_{xz}(k_{Fx}, 0) - \Sigma_{xz}(k_{Fy}, 0)}{k_F \partial_k \Sigma_{xz}(k, 0)|_{k=k_F}}. \quad (27)$$

In obtaining Eq. (26) we made the approximations

$$\mu - \varepsilon_{xz}(k_{Fx}) - \Sigma_{xz}(k_{Fx}, 0) \rightarrow \frac{\Sigma_{xz}(k_{Fy}, 0) - \Sigma_{xz}(k_{Fx}, 0)}{2} \quad (28)$$

and

$$\partial_{k_x} [\varepsilon_{xz}(\mathbf{k}) + \Sigma_{xz}(\mathbf{k}, 0)]|_{\mathbf{k}=k_{Fx}} \rightarrow \partial_k \Sigma_{xz}(k, 0)|_{k=k_F} \quad (29)$$

where $\partial_k \Sigma_{xz}(k, 0)$ is calculated using an alternative version of the t_{2g} 2DEG model *without anisotropy*. Specifically, for this particular quantity we use the isotropic version of Eq. (5):

$$\varepsilon_\alpha(\mathbf{k}) = \begin{cases} \frac{\hbar^2 \mathbf{k}^2}{2m_L} & \text{for } \alpha = xy, \sigma \\ \frac{\hbar^2 \mathbf{k}^2}{2m_{\text{DOS}}} + \Delta & \text{for } \alpha = xz, \sigma \\ \frac{\hbar^2 \mathbf{k}^2}{2m_{\text{DOS}}} + \Delta & \text{for } \alpha = yz, \sigma \end{cases} \quad (30)$$

The xz bands Fermi wavevector in this isotropic version is $k_F \equiv \sqrt{k_{Fx} k_{Fy}}$. Analogous approximations were carried out to obtain Eq. (27), and we have confirmed numerically that the large r_s asymptotic behavior appearing in Figure 3 is qualitatively unaltered by these approximations.

In a moment we will explain the differences in FSSM between the single-band anisotropic 2DEG and the xz band of the t_{2g} 2DEG by separately calculating the numerator and denominator of Eqs. (26) and (27) to leading-order in powers of $1/r_s$. First let us consider a simple scaling argument which highlights the critical role played by non-analyticity in the G_0W -RPA self-energy of the t_{2g} 2DEG. Consider the following series representation for the self-energy at zero frequency:

$$\Sigma_{xz}(\mathbf{k}, 0) = \frac{f(\mathbf{k})}{r_s^\alpha} + \frac{g(\mathbf{k})}{r_s^\beta} + \mathcal{O}\left(\frac{1}{r_s^\gamma}\right) + \dots \quad (31)$$

where $\alpha < \beta < \gamma$. We expect that the leading-order contribution to the numerator of Eqs. (26) and (27) comes from the leading-order term in Eq. (31) with a coefficient (*e.g.* $f(\mathbf{k})$ or $g(\mathbf{k})$) that actually depends on \mathbf{k} , as opposed to being a constant. Our calculations reveal that $\partial_k f(\mathbf{k}) = 0$ for both the xz band of the t_{2g} 2DEG and the single-band anisotropic 2DEG, and therefore the leading-order contribution to the numerator of Eqs. (26) and (27) comes from the sub-leading term in Eq. (31):

$$\Sigma_{xz}(k_{Fy}, 0) - \Sigma_{xz}(k_{Fx}, 0) \sim \frac{g(k_{Fy}) - g(k_{Fx})}{r_s^\beta}. \quad (32)$$

If the G_0W -RPA self-energy (*i.e.* $g(\mathbf{k})$) is analytic for \mathbf{k} on the non-interacting Fermi surface, then we can obtain the leading-order term in the $1/r_s$ series expansion for the denominators of Eqs. (26) and (27) directly from Eq. (31). This gives

$$k_F \partial_k \Sigma_{xz}(k, 0)|_{k=k_F} \sim \frac{g(k_F)}{r_s^\beta}, \quad (33)$$

where we have approximated the wavevector derivative of the self-energy by dividing through by the Fermi wavevector k_F . When Eqs. (32) and (33) are substituted into Eqs. (26) and (27) we obtain a constant,

$$\frac{\delta k_{Fx}}{k_{Fx}} = -\frac{\delta k_{Fy}}{k_{Fy}} = \frac{g(k_{Fy}) - g(k_{Fx})}{2g(k_F)}, \quad (34)$$

which while describing perfectly the saturation of FSSM in the single-band anisotropic 2DEG at large r_s , fails to describe the t_{2g} 2DEG. As we show explicitly below, the leading-order contribution to the wavevector dependent part of the G_0W -RPA self-energy of the xz band of the t_{2g} 2DEG is not analytic at the Fermi surface, and therefore the simple arguments leading to Eq. (34) do not apply in this case. The origin of this divergence is the long-range of the Coulomb interaction, and is similar to the divergence of the quasiparticle effective mass within Hartree-Fock theory²⁰.

We begin by calculating the denominator of Eqs. (26) and (27) for the single-band 2DEG. Putting wavevectors and frequencies in units of k_F and $\hbar k_F^2/m_{\text{DOS}}$, respectively, we obtain

$$\begin{aligned} \partial_k \Sigma(k, 0)|_{k=k_F} &= \left(\frac{2a_{\text{BRy}}}{\pi^2 \kappa} \right) \int_0^\infty q dq \int_{-\pi}^\pi d\theta \int_0^\infty d\Omega \\ &\times \frac{1/q}{1 + \frac{2^{1/2} r_s}{q} \chi^{(0)}(q, i\Omega)} \left(\frac{2q \cos[\theta] - 2}{\{q^2 - 2q \cos[\theta] + 2i\Omega\}^2} \right), \end{aligned} \quad (35)$$

where we have removed the xz subscript from the self-energy to explicitly indicate we are here considering the single-band 2DEG. The dimensionless Lindhard function $\chi^{(0)}(q, i\Omega)$ is obtained from the dimensionful form²⁰ by dividing out the negative density-of-states. We must now consider how to extract the leading-order in powers of $1/r_s$ term in Eq. (35). Physically speaking, a quasiparticle at momentum $\hbar \mathbf{k}$ and energy $\hbar \omega$ acquires its self-energy by making virtual transitions to intermediate states of momentum $\hbar \mathbf{k} - \hbar \mathbf{q}$ and energy $\hbar \omega - \hbar \Omega$, and back. This picture is motivated by the Feynman diagram for the G_0W -RPA self-energy and its mathematical representation, Eq. (15). The available phase-space for virtual transitions in which the momentum and energy transferred is on the order of the Fermi momentum and Fermi energy, respectively, scales like $k_F^4 \propto 1/r_s^4$, and vanishes swiftly in the limit of low density. Therefore the leading-order in powers of $1/r_s$ term from Eq. (35) instead comes from $|q| \gg 1$ and $\Omega \gg 1$. In this limit the dimensionless Lindhard function has a particularly

simple form²⁰

$$\chi^{(0)}(q, i\Omega) \rightarrow \frac{2q^2}{q^4 + 4\Omega^2}. \quad (36)$$

After expanding Eq. (35) to leading-order in the small parameter $\cos(\theta)/q$ we obtain an expression which can be evaluated analytically. We then find

$$\partial_k \Sigma(k, 0)|_{k=k_F} = \left(\sqrt{\frac{2}{\pi}} \frac{\Gamma[\frac{1}{3}] \Gamma[\frac{7}{6}] a_B \text{Ry}}{\kappa} \right) \frac{1}{r_s^{1/3}} \quad (37)$$

where $\Gamma[x]$ is the Euler gamma function. Next we evaluate the numerator of Eqs. (26) and (27) for the single-band anisotropic 2DEG. Following similar steps, and expanding the self-energy to leading-order in $\zeta \equiv m_H/m_L$ about $\zeta = 1$ we obtain

$$\begin{aligned} \Sigma(k_{Fy}, 0) - \Sigma(k_{Fx}, 0) &= - \left(\frac{8 \Gamma[\frac{7}{6}] \Gamma[-\frac{8}{3}] \bar{m}_{\text{DOS}} \text{Ry}}{81 \sqrt{\pi} \kappa^2} \right) \\ &\times \frac{\zeta - 1}{r_s^{4/3}}, \end{aligned} \quad (38)$$

where $\bar{m}_{\text{DOS}} = m_{\text{DOS}}/m$ and m is the bare electron mass in vacuum. We have successfully compared both Eqs. (37) and (38) against the full G_0W -RPA numerical calculations, and when these expressions are substituted into Eqs. (26) and (27) we confirm that FSSM in the single-band anisotropic 2DEG saturates at large r_s .

Let us now move on to considering the leading-order in $1/r_s$ expressions for the numerator and denominator of Eqs. (26) and (27) for the xz band of the t_{2g} 2DEG. Once again, phase-space considerations for virtual transitions suggest that the most important $\hbar\mathbf{q}$ and $\hbar\Omega$ are large on the scale of the xz band's Fermi momentum and Fermi energy, respectively. As a result, the RPA screened Coulomb interaction is accurately approximated by a simplified version of the dielectric function given in Eq. (14) which neglects $\chi_{xz}^{(0)}(q, i\Omega)$ and $\chi_{yz}^{(0)}(q, i\Omega)$ compared to $\chi_{xy}^{(0)}(q, i\Omega)$. It is useful to define the dimensionless interaction parameter R_s , which is analogous to Eq. (24) but describes the density in the xy band

$$n_{xy} = \frac{1}{\pi (a_{Bxy}^* R_s)^2}. \quad (39)$$

Here $a_{Bxy}^* = \kappa a_B/m_L$ defines the effective Bohr radius appropriate for the xy band. In the limit of a large energy offset, Δ , between the bottom of the xz and yz bands and the bottom of the xy band (*i.e.* $R_s \ll 1$), we are justified in approximating $\chi_{xy}^{(0)}(q, i\Omega)$ by its long wavelength limit. As detailed in the Appendix, we then find

$$\begin{aligned} \partial_k \Sigma_{xz}(k, 0)|_{k=k_F} &= - \left(\frac{a_B m_L \text{Ry}}{2\pi \kappa m_{\text{DOS}}} \right) \\ &\times \frac{R_s}{r_s} \ln \left[\frac{\kappa^2}{2\bar{m}_L} \Delta + \frac{m_{\text{DOS}}}{m_L} \frac{1}{r_s^2} \right] \end{aligned} \quad (40)$$

where Δ is in units of Rydbergs and $\bar{m}_L = m_L/m$. Similar approximations allow us to evaluate the numerator of Eqs. (26) and (27):

$$\Sigma_{xz}(k_{Fy}, 0) - \Sigma_{xz}(k_{Fx}, 0) = \left(\frac{2^{3/2} \bar{m}_{\text{DOS}} \text{Ry}}{\pi^2 \kappa^2} \right) \mathcal{F}(\zeta) \frac{R_s}{r_s^2} \quad (41)$$

where the function $\mathcal{F}(\zeta)$ can be written in terms of complete elliptic integrals and is given explicitly in the Appendix. After substituting Eqs. (40) and (41) into Eqs. (26) and (27) we find that FSSM in the elliptical bands of the t_{2g} 2DEG grows (sublinearly) with increasing r_s until the density in these bands is so low that $m_{\text{DOS}}/(m_L r_s^2) \ll \kappa^2 \Delta / (2\bar{m}_L)$, at which point FSSM in the elliptical bands of the t_{2g} 2DEG also saturates. Numerical calculations show that FSSM of the elliptical bands does indeed saturate for values of r_s much greater than those shown in Figure 3. The presence of the logarithmic factor in Eq. (40) is a signature of the non-analyticity of the xz band's G_0W -RPA self-energy when $R_s \ll 1$, and gives a simple explanation for FSSM in the elliptical bands of the t_{2g} 2DEG when r_s is large.

C. Self-consistent calculation of FSSM

Finally, to confirm the FSSM results in Section IV A, and also to check the validity of assuming that FSSM is small, we solve for the xz band's renormalized Fermi surface by self-consistently solving the two equations

$$\mu = \varepsilon_{xz}(k_{Fx}^*) + \text{Re} \Sigma_{xz}(k_{Fx}^*, 0) \quad (42)$$

and

$$\mu = \varepsilon_{xz}(k_{Fy}^*) + \text{Re} \Sigma_{xz}(k_{Fy}^*, 0). \quad (43)$$

The numerical solution follows simply by iteratively solving the above two equations while forcing the \mathbf{k} -space area of the xz band to remain constant. In the top and bottom panels of Fig. 4 we plot k_{Fx}^*/k_{Fx} and k_{Fy}^*/k_{Fy} versus r_s . Clearly the conclusions of Section IV A are confirmed.

We now turn our attention to understanding how interactions effect the quasiparticle effective mass.

V. QUASIPARTICLE EFFECTIVE MASS

Just as the free-space electron mass is renormalized by the periodic crystal potential of a solid, it can further be renormalized by the presence of electron-electron interactions^{19,20}. In both cases, the renormalized mass is defined so that the single-particle excitation energies are well approximated by the non-interacting kinetic energy formula with the bare mass replaced by the renormalized mass. In the t_{2g} 2DEG, the effect of the crystal potential is already captured by Eq. (5). To evaluate the effect of

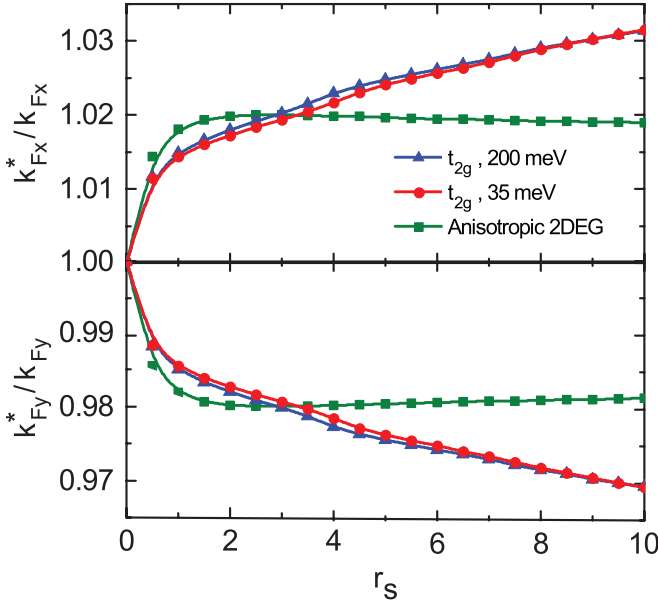


FIG. 4: (Color online) Same as Fig. 3, but calculated by the self-consistent solution of Eqs. (42) and (43), rather than using the linearized Eqs. (26)-(27).

electron-electron interactions on the t_{2g} 2DEG quasiparticle mass values, we expand the quasiparticle excitation energy about the renormalized Fermi surface:

$$\mathcal{E}_\alpha(\mathbf{k}) = (\mathbf{k} - \mathbf{k}_{F\alpha}^*) \cdot \nabla_{\mathbf{k}} \mathcal{E}_\alpha(\mathbf{k})|_{\mathbf{k}=\mathbf{k}_{F\alpha}^*} + \mathcal{O}(\delta k^2). \quad (44)$$

We focus on the quasiparticle mass of the xz band for which the \hat{x} -direction bare mass is m_L (including the effect of the periodic crystal potential but not yet including electron-electron interactions) and the \hat{y} -direction bare mass is m_H .

The renormalized light and heavy masses can be calculated using

$$m_L^* = \frac{\hbar^2 k_{Fx}^*}{[d\mathcal{E}_{xz}(\mathbf{k})/dk_x]_{\mathbf{k}=\mathbf{k}_{Fx}^*}} \quad (45)$$

and

$$m_H^* = \frac{\hbar^2 k_{Fy}^*}{[d\mathcal{E}_{xz}(\mathbf{k})/dk_y]_{\mathbf{k}=\mathbf{k}_{Fy}^*}}. \quad (46)$$

Using Eq. (6) relating the quasiparticle energy to the self-energy, we find the following relationship between the self-energy and the quasiparticle masses,

$$\frac{m_L^*}{m_L} = \frac{1 - \hbar^{-1} \partial_\omega \text{Re} \Sigma_{xz}(k_{Fx}^*, \omega)|_{\omega=0}}{1 + (m_L/\hbar^2 k_{Fx}^*) \partial_{k_x} \text{Re} \Sigma_{xz}(\mathbf{k}, 0)|_{\mathbf{k}=\mathbf{k}_{Fx}^*}} \quad (47)$$

and

$$\frac{m_H^*}{m_H} = \frac{1 - \hbar^{-1} \partial_\omega \text{Re} \Sigma_{xz}(k_{Fy}^*, \omega)|_{\omega=0}}{1 + (m_H/\hbar^2 k_{Fy}^*) \partial_{k_y} \text{Re} \Sigma_{xz}(\mathbf{k}, 0)|_{\mathbf{k}=\mathbf{k}_{Fy}^*}}. \quad (48)$$

The right-hand-sides of these equations can be evaluated using the G_0W -RPA approximation for the self-energy.

A. Quasiparticle effective mass at high densities

Before presenting our numerical results, we briefly consider the high-density (small r_s) limit where analytic results for the quasiparticle mass can be obtained. These results will offer insight into the physical processes which renormalize the electron mass.

We start by simplifying the t_{2g} model slightly to make the derivation tractable. We take the xz and yz bands to be isotropic with mass $m_{\text{DOS}} = \sqrt{m_H m_L}$ as in Eq. (30). The influence of anisotropy on the quasiparticle mass is isolated and studied in Section VB, but we neglect it here. In this section it is advantageous to work with the zero-temperature formalism of many-body perturbation theory⁴¹. In units of effective Rydbergs, $\text{Ry}^* = (m_{\text{DOS}}/\kappa^2)\text{Ry}$, the G_0W -RPA self-energy of the xz band is

$$\begin{aligned} \Sigma_{xz}(\mathbf{k}, \omega) &= -\frac{\sqrt{2}}{\pi r_s} \int d^2 \mathbf{q} \int_{-\infty}^{\infty} \frac{d\Omega}{2\pi i} W_{xz}(\mathbf{q}, \Omega) \\ &\times G_{xz}^{(0)}(\mathbf{k} + \mathbf{q}, \omega + \Omega), \end{aligned} \quad (49)$$

where we are now using dimensionless frequencies (ω, Ω) and wavevectors (\mathbf{q}, \mathbf{k}) by expressing them in units of $2\varepsilon_{F_{xz}}/\hbar$ and $k_{F_{xz}}$, respectively. We define r_s here as in Eq. (39). The dimensionless Green's function is

$$G_{xz}^{(0)}(\mathbf{k} + \mathbf{q}, \omega + \Omega) = \frac{1}{\omega + \Omega - \left(\frac{|\mathbf{k} + \mathbf{q}|^2}{2} + \bar{\Delta}\right) + i\eta} \quad (50)$$

where the limit $\eta \rightarrow 0^+$ is implied for $|\mathbf{k} + \mathbf{q}| > k_{F_{xz}}$ and $\eta \rightarrow 0^-$ for $|\mathbf{k} + \mathbf{q}| < k_{F_{xz}}$. Here $\bar{\Delta}$ is the band offset between the xz and yz bands and the xy band in units of $2\varepsilon_{F_{xz}}$. Recent tight-binding calculations²¹ of SrTiO₃ heterostructures suggest that the spatial separation d becomes small at large electron densities. In the limit $k_{F_{xz}}d \ll 1$, the dimensionless RPA screened interaction of Eq. 13 reduces to

$$\frac{1}{q + \sqrt{2}r_s \left[\zeta^{-1/2} \chi_{xy}^{(0)}(\lambda q, \lambda^2 \Omega) + \chi_{yz}^{(0)}(q, \Omega) + \chi_{xz}^{(0)}(q, \Omega) \right]} \quad (51)$$

where we have defined $\lambda = k_{F_{xz}}/k_{F_{xy}}$ and $\zeta = m_H/m_L$ has been introduced earlier. The density-response functions, $\chi_\alpha^{(0)}$, are dimensionless here and are obtained from the dimensional functions²⁰ by dividing by the negative density-of-states of the α 'th band.

Since the kinetic energy scales as $1/r_s^2$ and the Coulomb interaction energy scales as $1/r_s$, electron gases are weakly interacting in the high density (small r_s) limit. We are then justified in ignoring the self-consistent nature of Eq. (6) for the quasiparticle excitation energy and we can apply the ‘‘on-shell’’ approximation

$$\mathcal{E}_{xz}(k) \simeq \varepsilon_{xz}(k) + \text{Re} \Sigma_{xz}(k, \varepsilon_{xz}(k)/\hbar) - \mu. \quad (52)$$

The inverse of the xz band's quasiparticle mass enhance-

ment factor is then given by

$$\frac{m_{xz}}{m_{xz}^*} = 1 + \frac{r_s^2}{4} \left[\frac{\partial}{\partial k} \text{Re} \Sigma_{xz}(k, \varepsilon_{xz}(k)) \right]_{k=1}. \quad (53)$$

To evaluate the wavevector derivative of the self-energy we need the derivative of the Green's function. Evaluating this on the Fermi surface we find

$$\begin{aligned} & \left. \frac{\partial}{\partial k} G_{xz}^{(0)}(\mathbf{k} + \mathbf{q}, \varepsilon(k) + \Omega) \right|_{k=1} \\ &= -2\pi i \delta(1 - |\hat{\mathbf{k}} + \mathbf{q}|) \delta(\Omega) \left[(\hat{\mathbf{k}} + \mathbf{q}) \cdot \hat{\mathbf{k}} \right] \\ &+ (\hat{\mathbf{k}} \cdot \mathbf{q}) \left[G_{xz}^{(0)}(\hat{\mathbf{k}} + \mathbf{q}, \varepsilon(1) + \Omega) \right]^2, \end{aligned} \quad (54)$$

where $\hat{\mathbf{k}} = \mathbf{k}/k$ is a unit vector. The first term on the right-hand side of Eq. (54) gives the leading order in r_s contribution to the quasiparticle mass. The remaining integrations in Eq. (49) can be performed analytically. After substituting the result into Eq. (53), we obtain the inverse quasiparticle mass to $\mathcal{O}(r_s)$:

$$\frac{m_{xz}}{m_{xz}^*} = 1 - \frac{r_s}{\pi\sqrt{2}} \ln\left(\frac{r_s\delta}{2\sqrt{2}}\right) - \frac{\sqrt{2}r_s}{\pi} \quad (55)$$

where $\delta \equiv (\zeta^{-1/2} + 2)$. The expression appropriate to a single-band 2DEG is found by taking the limit $\delta \rightarrow 1$, which we have confirmed by comparing with full G_0W -RPA numerical calculations. The effective mass enhancement factor, which is given by the inverse of Eq. (55), is shown in Fig. 5.

As the inset to Fig. 5 shows, the small r_s expression (55) is only quantitatively useful for $r_s \lesssim 0.1$. It does, however, offer useful qualitative insight into the role of screening on the quasiparticle mass. Physically, the renormalization of the electron mass derives from screened exchange scattering processes (see Fig. 2) between the quasiparticle whose mass is under investigation, and other quasiparticles in the Fermi sea. Because of the Dirac delta functions in Eq. (54), the leading order contribution comes from scattering amongst quasiparticles restricted to the Fermi surface, just as in the three-dimensional electron gas^{43,44}. For this reason, the presence of electrons in the xy and yz bands enters Eq. (55) only through their band-resolved density-of-states evaluated at the Fermi surface. The xy band's finite density-of-states contributes the factor $\zeta^{-1/2}$ in the definition of δ , while the yz band's density-of-states contributes half of the factor of 2 in the definition of δ (the other half comes from screening by the xz band's own electrons).

If we identify the above derivation as a simple application of first-order perturbation theory, but with the unscreened Coulomb interaction replaced with a Thomas-Fermi (TF) screened interaction²⁰ (to which it is indeed equivalent), then we can understand in simple terms how increased screening acts to increase the quasiparticle mass. First consider that we know the exchange contribution to the self-energy tends to reduce the effective mass (in fact, the exchange level self-energy yields

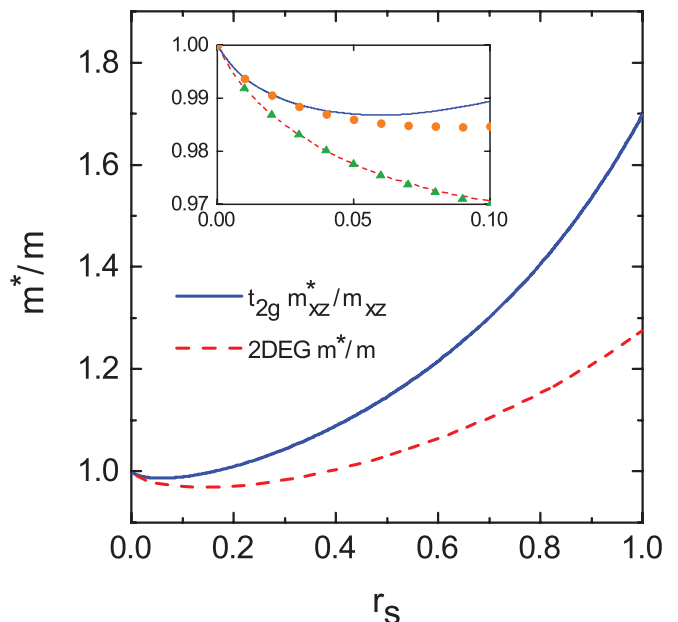


FIG. 5: (Color online) The leading-order-in- r_s quasiparticle mass enhancement factor (*i.e.* the inverse of Eq. (55)) is plotted for $r_s < 1$. The dashed red line shows the result for a isotropic single-band 2DEG, and the solid blue line shows the result for the xz -band of the t_{2g} 2DEG, which also includes the effect of screening by electrons in the yz and xy bands. The Thomas-Fermi screened electron-electron interaction gives the leading-order contribution to quasiparticle mass enhancement at small r_s (high density). The presence of multiple filled bands in the t_{2g} 2DEG yields a larger Thomas-Fermi screening wavevector, and therefore a larger quasiparticle mass enhancement than in a single-band 2DEG.

quasiparticles with *zero* effective mass), so if a increase in the screening wavevector acts to reduce the exchange energy, then it will also have the effect of enhancing the quasiparticle mass. The unscreened exchange self-energy in Eq. (19) for an electron of wavevector \mathbf{k} is a sum over occupied states \mathbf{q} of the bare amplitude $v_{|\mathbf{k}-\mathbf{q}|} = 2\pi e^2/(\kappa|\mathbf{k}-\mathbf{q}|)$. When we include a TF screening wavevector κ_{TF} (which is proportional to the total density-of-states at the Fermi surface), the bare amplitude is replaced by $v_{|\mathbf{k}-\mathbf{q}|} \rightarrow 2\pi e^2/(\kappa|\mathbf{k}-\mathbf{q}| + \kappa_{\text{TF}})$, which is smaller for all values of \mathbf{q} to be summed over. Indeed, the larger κ_{TF} is (more specifically, the more electrons present at the Fermi surface), the smaller the TF self-energy. It is in this way that the xy and yz band's electrons act to increase the xz band's quasiparticle masses.

B. The role of anisotropy

Before presenting our numerical results for the t_{2g} 2DEG, let us illustrate the general effect of band anisotropy on the quasiparticle mass in a simpler case. To separate out this effect, we consider a single-band

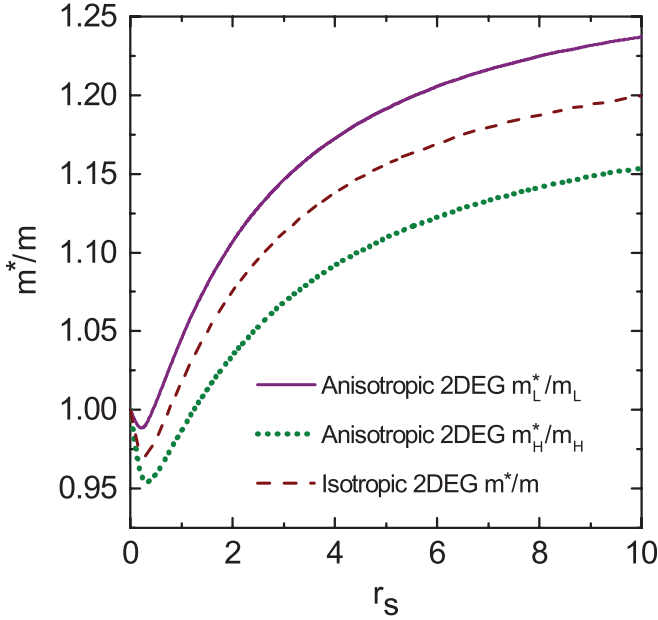


FIG. 6: (Color online) The quasiparticle mass enhancement factor of a isotropic single-band 2DEG (brown dashed line) compared against the light (purple) and heavy (green) quasiparticle mass enhancement factors of an anisotropic single-band 2DEG.

anisotropic 2DEG with the following non-interacting band structure

$$\varepsilon(\mathbf{k}) = \frac{\hbar^2 k_x^2}{2m_L} + \frac{\hbar^2 k_y^2}{2m_H}. \quad (56)$$

We define the heavy and light quasiparticle mass factors m_H^*/m_H and m_L^*/m_L as above, and plot them in Fig. 6 against r_s . Here r_s is defined as in Eq. (39) but with n_{xz} replaced by the total density of the single band. We also plot the quasiparticle mass factor m^*/m for an isotropic two-dimensional electron gas for comparison. We find that m_L^*/m_L (m_H^*/m_H) is enhanced (reduced) compared to the isotropic 2DEG mass enhancement factor m^*/m at all values of r_s , or equivalently, total 2DEG density.

To understand these results it is again helpful to consider the small r_s regime where the effective mass enhancement is governed by the TF screened self-energy. Consider first a single isotropic band with dispersion $\varepsilon(k) = \hbar^2 \mathbf{k}^2 / (2m_{\text{DOS}})$ where as defined above $m_{\text{DOS}} = \sqrt{m_H m_L}$. The isotropic 2DEG mass enhancement factor in the TF approximation can be written as

$$\frac{m_{\text{DOS}}^*}{m_{\text{DOS}}} = \frac{1}{1 + \delta v_{\text{F}}^* / v_{\text{F}}}, \quad (57)$$

where $v_{\text{F}} = \hbar k_{\text{F}} / m_{\text{DOS}}$ is the non-interacting band velocity at the Fermi energy, and the interaction contribution to the renormalized quasiparticle velocity at the Fermi energy is given by

$$\delta v_{\text{F}}^* = v_{\text{F}}^* - v_{\text{F}} = \hbar^{-1} [\partial_{\mathbf{k}} \Sigma^{\text{TF}}(\mathbf{k})]_{\mathbf{k}=\mathbf{k}_{\text{F}}}. \quad (58)$$

The TF self-energy of a single-band isotropic 2DEG is given by

$$\Sigma^{\text{TF}}(\mathbf{k}) = -\frac{1}{(2\pi)^2} \int d^2 \mathbf{q} \frac{2\pi e^2}{\kappa (|\mathbf{k} - \mathbf{q}| + \kappa_{\text{TF}})} \times \Theta\{\varepsilon_{\text{F}} - \varepsilon(\mathbf{q})\} \quad (59)$$

where the TF screening wavevector is defined

$$\kappa_{\text{TF}} = \frac{2\pi e^2}{\kappa} N(0). \quad (60)$$

Here $N(0)$ is the total density-of-states at the Fermi surface. The quasiparticle mass enhancement factor calculated in this way is shown in Fig. 5. Next consider keeping the density (r_s) constant while introducing anisotropy in this single-band 2DEG by slowly deforming the shape of the Fermi surface from a circle to an ellipse with semimajor (semiminor) axes $k_{\text{F}y}$ ($k_{\text{F}x}$). The non-interacting dispersion of the anisotropic band is given by $\varepsilon(\mathbf{k}) = \hbar^2 k_x^2 / (2m_L) + \hbar^2 k_y^2 / (2m_H)$ and the TF approximation for the light quasiparticle mass enhancement factor m_L^*/m_L can be found from Eq. (57) by replacing $v_{\text{F}} = \hbar k_{\text{F}} / m_{\text{DOS}}$ with $v_{\text{F}x} = \hbar k_{\text{F}x} / m_L$, and also replacing $\delta v_{\text{F}}^* = \hbar^{-1} [\partial_{\mathbf{k}} \Sigma^{\text{TF}}(\mathbf{k})]_{\mathbf{k}=\mathbf{k}_{\text{F}}}$ with $\delta v_{\text{F}x}^* = \hbar^{-1} [\partial_{k_x} \Sigma^{\text{TF}}(\mathbf{k})]_{\mathbf{k}=\mathbf{k}_{\text{F}x}}$:

$$\frac{m_L^*}{m_L} = \frac{1}{1 + \delta v_{\text{F}x}^* / v_{\text{F}x}}. \quad (61)$$

By examining separately how the introduction of band anisotropy changes $\delta v_{\text{F}x}^*$ relative to δv_{F}^* , and $v_{\text{F}x}$ relative to v_{F} , we can identify the most important factor leading to $m_L^*/m_L > m_{\text{DOS}}^*/m_{\text{DOS}}$ for a given r_s . Because the quasiparticle state at the Fermi surface in the light mass direction ($k_x = k_{\text{F}x}$, $k_y = 0$) has more occupied states near it in momentum space when anisotropy is present, the TF self-energy of this state is increased in magnitude. Furthermore, since the TF self-energy acts to increase the quasiparticle velocity (*i.e.* decrease the quasiparticle mass, as shown in the previous section), it follows that $\delta v_{\text{F}x}^* > \delta v_{\text{F}}^*$. Thus electron-electron interactions tend to reduce m_L^*/m_L below $m_{\text{DOS}}^*/m_{\text{DOS}}$ for a given value of r_s . Despite this, the opposite occurs in Fig. 6. The reason is that the band velocity $v_{\text{F}x} = \hbar k_{\text{F}x} / m_L$ also enters the expression for the quasiparticle mass enhancement factor m_L^*/m_L , and for a fixed density we find $v_{\text{F}x} > v_{\text{F}}$, which tends to enhance m_L^*/m_L above $m_{\text{DOS}}^*/m_{\text{DOS}}$. This latter effect is larger, and so while the change in quasiparticle velocity in the light mass direction is increased by anisotropy, the accompanying increase in band velocity is larger and results in $m_L^*/m_L > m_{\text{DOS}}^*/m_{\text{DOS}}$ for a given r_s . Analogous reasoning leads to the conclusion that $m_H^*/m_H < m_{\text{DOS}}^*/m_{\text{DOS}}$ for a given r_s . Although analysis based on the TF self-energy can only be guaranteed to hold at small r_s , the conclusions it gives clearly persist within the full G_0W -RPA results of Fig. 6 to large r_s .

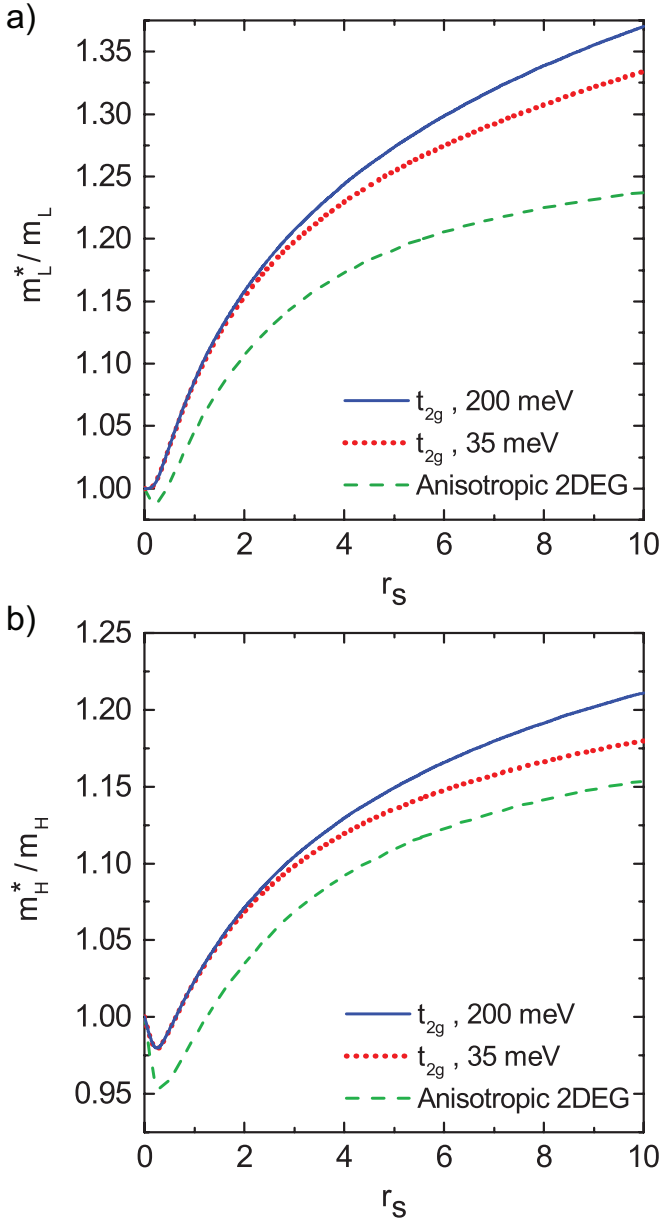


FIG. 7: (Color online) Panel (a) shows the light quasiparticle mass of the t_{2g} 2DEG's xz band plotted against r_s for several values of the band offset Δ and separation d . For the red curve $\Delta = 35$ meV and $d = 10a$ where $a = 3.9$ Å is the SrTiO₃ lattice constant. For the blue curve $\Delta = 200$ meV and $d = 2a$. The dashed green curve is for a single-band anisotropic 2DEG whose \hat{x} -direction and \hat{y} -direction non-interacting masses are the same as the xz band in the t_{2g} model. For this curve r_s is defined from the total density in the single anisotropic band. Panel (b) is the same, but for the heavy effective mass.

C. The t_{2g} Quasiparticle Mass

In this section we present the results of our numerical calculation of the G_0W -RPA effective masses m_H^* and m_L^* of the xz anisotropic band in the t_{2g} 2DEG model. The results for the yz band are identical because of symmetry.

In Fig. 7 we compare the quasiparticle masses in the t_{2g} 2DEG against those in a single-band anisotropic 2DEG with a non-interacting energy dispersion as in Eq. (56). Tight-binding studies of the t_{2g} 2DEG created at SrTiO₃ surfaces or heterojunctions reveal that as the confining potential increases, so does the energy offset parameter Δ , while the distance separating the xy band from the xz and yz bands d decreases²¹. We have included in Fig. 7 results for the t_{2g} quasiparticle masses in the case of the very highest t_{2g} electron densities ($\Delta = 200$ meV and $d = 2a$ where $a = 3.9$ Å) as well as for the lowest t_{2g} electron densities ($\Delta = 35$ meV and $d = 10a$) at which we might practically neglect the presence of spin-orbit coupling in SrTiO₃ and thus reliably apply the t_{2g} 2DEG model introduced in Sect. II. In agreement with our analytic results in Section V A, the quasiparticle masses in the t_{2g} 2DEG are appreciably larger than their counterparts in the single-band anisotropic 2DEG.

We were able to show in Sect. V A that at small r_s the increased quasiparticle mass in the anisotropic bands of the t_{2g} 2DEG followed from a suppression of the wavevector derivative of the quasiparticle self-energy, which itself followed from an increase in the electronic screening of interactions due to the presence of electrons in the other bands (i.e. the xy and yz bands). In that calculation we discovered that, at leading order in r_s , the quasiparticle mass comes from exchange scattering via a reduced interaction in the form of the TF screened Coulomb interaction. Thus at small r_s , because we knew that the additional electrons in the xy and yz bands would increase the TF screening wavevector, we knew the quasiparticle mass would be enhanced in the t_{2g} 2DEG. In confirmation of this derivation, our numerical calculations reveal a substantial reduction in the wavevector derivative of the xz bands self-energy when other bands are occupied. This reduction increases for increasing r_s . At larger values of r_s , however, correlation effects become important. Indeed, Eqs. (47) and (48), which define the quasiparticle masses, depend on the frequency derivative of the self-energy as well. Note that the self-energy is frequency independent in Hartree-Fock, and thus frequency dependence manifestly represents a correlation effect. Furthermore, we note that the frequency dependence of the self-energy does not enter the lowest order in r_s expressions for the quasiparticle mass derived in Sect. V A, as in this limit interactions are weak compared to the kinetic energy, and first-order perturbation theory is here equivalent to Hartree-Fock. Numerically, we find that the frequency derivative of the xz bands quasiparticle self-energy is also suppressed by the presence of electrons in the xy and yz bands. Since the frequency and wavevector derivatives both are suppressed, some degree of cancellation occurs in Eqs. (47) and (48) for the t_{2g} quasiparticle masses. Despite this, we find that the quasiparticle masses of the t_{2g} anisotropic bands are enhanced from 25 to 75 percent above the quasiparticle mass values in a single-band anisotropic 2DEG.

VI. SUMMARY AND DISCUSSION

Motivated by the recent synthesis of transition-metal oxide two-dimensional electron gases, we have introduced a model for studying the effects of many-body interactions in these systems. Using information from recent tight-binding^{21,22} and *ab initio* calculations²³⁻²⁵ we have chosen model parameters to specifically describe the electron gas formed in SrTiO₃. Our model captures the presence of band anisotropy, energy offsets between bands, and variable band confinement at the interface, all of which are characteristics likely to be shared by any two-dimensional electron gases formed from d-orbitals with anisotropic nearest-neighbor hopping amplitudes. Because the average conduction electron occupation number per transition-metal site is much less than one, the full long-range Coulomb interaction must be retained in any realistic interacting-electron model. Our approach satisfies this criterion.

We have used the G_0W -RPA approximation to calculate the self-energy contribution to the quasiparticle energy of the xz and yz anisotropic bands of the t_{2g} two-dimensional electron gas. Because these bands' constituent d-orbitals have a large hopping amplitude in one direction in-plane and a small hopping amplitude in the other, the two-dimensional Fermi surfaces of these bands are approximately elliptical. Because rotational symmetry is broken, the self-energy depends on the quasiparticle wavevector's orientation in momentum space, and the Fermi surface shape can be renormalized by interactions. By comparing the degree of Fermi surface renormalization in the anisotropic bands of the t_{2g} model to the single-band anisotropic two-dimensional electron gas, we identified the reduction in band anisotropy as a rather universal effect, likely to occur in any anisotropic electron gas with long-range Coulomb interactions.

Next we studied the impact of Coulomb interactions on the quasiparticle masses of the anisotropic bands in the t_{2g} 2DEG model. We derived an analytic expression for the high-density (small r_s) effective mass in both the t_{2g} electron gas and the ordinary single-band isotropic two-dimensional electron gas. This leading order in r_s contribution to the two-dimensional quasiparticle mass was found to arise from exchange scattering via a reduced electron-electron interaction in the form of a TF screened Coulomb potential. The presence of multiple bands in the t_{2g} case increased the TF screening wavevector, which substantially increased the quasiparticle masses m_H^* and m_L^* . Numerical calculations at larger values of r_s confirm that the additional screening present in the t_{2g} system from the multiple occupied bands increases the quasiparticle mass by reducing the wavevector dependence of the self-energy.

While the degree of Fermi surface shape renormalization is small and perhaps difficult to observe experimen-

tally, the quasiparticle mass of the t_{2g} anisotropic bands shows a large enhancement over the values expected in single-component 2DEGs. Shubnikov-de Haas oscillations are sensitive to the quasiparticle mass^{20,34-36}, but to our knowledge no clear signatures of the anisotropic band's Fermi surfaces have been reported in SrTiO₃ two-dimensional electron gases⁴⁵. When the mass is large, Landau-level spacing is small. It may be so small that disorder in current samples make oscillations attributable to the anisotropic bands undetectable. Perhaps the large quasiparticle mass we have found here helps to explain the lack of detection.

Acknowledgments

J.R.T. thanks the Scuola Normale Superiore di Pisa for their kind hospitality during part of this work. Work in Austin was supported by the DOE Division of Materials Sciences and Engineering under grant DE-FG02-ER45118.

Appendix A: Details of the Analytical calculation of FSSM in the t_{2g} 2DEG

In this appendix we outline the derivation of Eq. (40) and Eq. (41) from the main text. Let us begin with the former. We start using k_F to define dimensionless wavevectors and $\hbar k_F^2/m_{\text{DOS}}$ to define dimensionless frequencies. After expanding the wavevector derivative of the Green's function appearing in the G_0W -RPA expression for $\partial_k \Sigma(k, 0)|_{k=k_F}$ to leading-order in the small-parameter $\cos(\theta)/q$ we obtain

$$\begin{aligned} \partial_k \Sigma(k, 0)|_{k=k_F} &= \frac{-2a_B R_y}{\pi^2 \kappa} \int_0^\infty q dq \int_{-\pi}^\pi d\theta \int_0^\infty d\Omega \\ &\times \left(\frac{q^4 - 4\Omega^2}{\{q^4 + 4\Omega^2\}^2} \right) \left(\frac{1/q}{1 + \frac{\sqrt{2}r_s}{q} \left\{ \frac{m_L}{m_{\text{DOS}}} \chi_{xy}^{(0)}(q, i\Omega) \right\}} \right) \end{aligned} \quad (\text{A1})$$

where we have only written terms which will contribute at leading-order in powers of $1/r_s$ in the final expression. The factor of m_L/m_{DOS} appears in front of $\chi_{xy}^{(0)}(q, i\Omega)$ because the xy band has a smaller band-mass and therefore a smaller density-of-states compared to the xz and yz bands. For simplicity we have set the confinement separation distance to zero, $d = 0$, in the RPA screened interaction. We now rewrite the wavevector derivative of the self-energy using k_{Fxy} and $\hbar k_{Fxy}^2/m_{\text{DOS}}$ to define dimensionless wavevectors and frequencies, respectively. After this transformation it becomes clear that Eq. (A1) appears to scale like $1/r_s$. After introducing R_s and changing variables to $v = \Omega/q$ we find

$$\partial_k \Sigma(k, 0)|_{k=k_F} = \frac{-4m_{\text{DOS}} a_B R_y}{\pi \kappa m_L} \frac{R_s}{r_s} \int_0^\infty dq \int_0^\infty dv \left(\frac{1/q}{1 + \frac{\sqrt{2}R_s}{q} \chi_{xy}^{(0)}(q, iqv)} \right) \left(\frac{q^2 - 4 \left(\frac{m_{\text{DOS}}}{m_L} \right)^2 v^2}{\left\{ q^2 + 4 \left(\frac{m_{\text{DOS}}}{m_L} \right)^2 v^2 \right\}^2} \right) \quad (\text{A2})$$

In the limit of $R_s \ll 1$ we can approximate the Lindhard function along the imaginary frequency axis by its long-wavelength limit

$$\lim_{q \rightarrow 0} \chi_{xy}^{(0)}(q, iqv) = 1 - \frac{v}{\sqrt{v^2 + 1}}. \quad (\text{A3})$$

When Eq. (A3) is inserted into Eq. (A2), we find that the integral diverges like $1/v$ in the long-wavelength limit. This is not surprising considering we have taken the large Ω and q limit in obtaining Eq. (A2). The analytic properties of the Lindhard function provide us with a convenient small v (*i.e.* low energy) cutoff, v_c . Specifically, the Lindhard function is non-analytic²⁰ in the sense that the long-wavelength limit is different depending on whether $v > 1$ or $v < 1$. Careful examination of the Lindhard

functions for each band of the t_{2g} 2DEG indicates that for $v < 1$, screening from the elliptical xz and yz bands is important for convergence. Inclusion of these functions, however, leads to higher-order expressions in powers of $1/r_s$. For $v > 1$ meanwhile, screening from the elliptic bands can be completely neglected. Applying the low-energy cutoff $v_c = 1$, the remaining integrals can be completed to yield Eq. (40) in the main text.

The derivation of Eq. (41) from the main text proceeds along very similar steps, which we briefly outline now. Again we start by using k_F to define dimensionless wavevectors and $\hbar k_F^2/m_{\text{DOS}}$ to define dimensionless frequencies. After applying the coordinate transformation $k_x \rightarrow \zeta^{-1/4} k_x$, $q_x \rightarrow \zeta^{-1/4} q_x$, $k_y \rightarrow \zeta^{1/4} k_y$ and $k_y \rightarrow \zeta^{1/4} k_y$, we find

$$\begin{aligned} \Sigma_{xz}(k_{Fy}, 0) - \Sigma_{xz}(k_{Fx}, 0) &= \frac{-2^{3/2} \bar{m}_{\text{DOS}} R_y}{\pi^2 \kappa^2 r_s} \int_0^\infty dq \int_{-\pi}^\pi d\theta \int_0^\infty d\Omega \left(\frac{1}{\gamma_{yz} + \frac{\sqrt{2}r_s m_L}{q m_{\text{DOS}}} \chi_{xy}(\gamma_{yz} q, i\Omega)} \right) \\ &\times \left(\frac{2q \sin(\theta) - q^2}{4\Omega^2 + \{2q \sin(\theta) - q^2\}^2} - \frac{2q \cos(\theta) - q^2}{4\Omega^2 + \{2q \cos(\theta) - q^2\}^2} \right), \end{aligned} \quad (\text{A4})$$

where we define $\gamma_{xz} = \sqrt{\zeta^{1/2} \cos^2(\theta) + \zeta^{-1/2} \sin^2(\theta)}$ and $\gamma_{yz} = \sqrt{\zeta^{-1/2} \cos^2(\theta) + \zeta^{1/2} \sin^2(\theta)}$. After some simple algebraic manipulations, and expanding to order x^2 in the small parameter $x = \cos(\theta)/q$ (which is the first non-vanishing term in the expansion) we obtain

$$\begin{aligned} \Sigma_{xz}(k_{Fy}, 0) - \Sigma_{xz}(k_{Fx}, 0) &= \frac{8\sqrt{2} \bar{m}_{\text{DOS}}^3 R_y}{\pi^2 \kappa^2 \bar{m}_L^2} \frac{R_s}{r_s^2} \int_0^\infty dq \int_{-\pi}^\pi d\theta \int_0^\infty d\Omega \frac{q^8 - 12q^4 \left(\frac{m_{\text{DOS}}}{m_L} \right)^2 \Omega^2}{\left(q^4 + 4 \left(\frac{m_{\text{DOS}}}{m_L} \right)^2 \Omega^2 \right)^3} \cos^2(\theta) \\ &\times \left(\frac{1}{\gamma_{xz} + \frac{\sqrt{2}R_s}{q} \chi_{xy}(\gamma_{xz} q, i\Omega)} - \frac{1}{\gamma_{yz} + \frac{\sqrt{2}R_s}{q} \chi_{xy}(\gamma_{yz} q, i\Omega)} \right), \end{aligned} \quad (\text{A5})$$

where we are now using k_{Fxy} and $\hbar k_{Fxy}^2/m_{\text{DOS}}$ to define dimensionless wavevectors and frequencies, respectively. For $R_s \ll 1$ the leading-order term comes from $v > 1$ again. With this low-energy cutoff, Eq. (A5) remains convergent even when $R_s = 0$ in the denominator of the integrand. This allows us to evaluate the remaining integrals analytically and we finally obtain Eq. (41) from the main text. The function $\mathcal{F}(\zeta)$ in Eq. (41) is given by

$$\mathcal{F}(\zeta) = \frac{(1 + \zeta) \left(\sqrt{\zeta} K[1 - \zeta] + K \left[\frac{\zeta - 1}{\zeta} \right] \right)}{(\zeta - 1) \zeta^{1/4}} - \frac{(1 + \zeta) \left(2\sqrt{\zeta} E[1 - \zeta] + 2\zeta E \left[\frac{\zeta - 1}{\zeta} \right] \right)}{(\zeta - 1) \zeta^{1/4}} \quad (\text{A6})$$

where $K[x]$ and $E[x]$ are complete elliptic integrals of the first and second kind, respectively.

- * Electronic address: tolsma@physics.utexas.edu
- ¹ J. Hubbard, *Proc. R. Soc. Lond. A* **276**, 238 (1963).
 - ² L.F. Mattheiss, *Phys. Rev. B*, **6**, 4718 (1972).
 - ³ A.P. Kajdos, D.G. Ouellette, T.A. Cain and S. Stemmer *Appl. Phys. Lett.* **103**, 082120 (2013).
 - ⁴ Y. Kozuka, M. Kim, H. Ohta, Y. Hikita, C. Bell, and H.Y. Hwang, *Appl. Phys. Lett.* **97**, 222115 (2010).
 - ⁵ J. Mannhart and D.G. Schlom, *Science* **327**, 1607 (2010).
 - ⁶ S. Stemmer and S.J. Allen, *Annu. Rev. Mater. Res.* **44**, 151 (2014).
 - ⁷ J.A. Sulpizio, S. Ilani, P. Irvin, and J. Levy, *Annu. Rev. Mater. Res.* **44**, 117 (2014).
 - ⁸ P. Moetakef, C.A. Jackson, J. Hwang, L. Balents, S.J. Allen, and S. Stemmer, *Phys. Rev. B*, **86**, 201102(R) (2012).
 - ⁹ R. Chen, S. Lee, and L. Balents, *Phys. Rev. B*, **87**, 161119(R) (2013).
 - ¹⁰ D. Bohm and D. Pines, *Phys. Rev.* **92**, 609 (1953).
 - ¹¹ M. Jonson, *J. Phys. C: Solid State Phys.* **9**, 3055 (1976).
 - ¹² F. Stern, *Phys. Rev. Lett.* **18**, 546 (1967).
 - ¹³ D. Grecu, *J. Phys. C: Solid State Phys.* **8**, 2627 (1975).
 - ¹⁴ B. Vinter, *Phys. Rev. Lett.* **35**, 1044 (1975).
 - ¹⁵ G.E. Santoro and G.F. Giuliani, *Phys. Rev. B*, **39**, 12818 (1989).
 - ¹⁶ R. Asgari, B. Davoudi, M. Polini, G.F. Giuliani, M.P. Tosi, and G. Vignale, *Phys. Rev. B*, **71**, 045323 (2005).
 - ¹⁷ M. Polini, R. Asgari, G. Borghi, Y. Barlas, T. Pereg-Barnea and A. H. MacDonald, *Phys. Rev. B*, **77**, 081411(R) (2008).
 - ¹⁸ A. Bostwick, F. Speck, T. Seyller, K. Horn, M. Polini, R. Asgari, A. H. MacDonald and E. Rotenberg, *Science* **328**, 999 (2010).
 - ¹⁹ D. Pines and P. Nozières, *The Theory of Quantum Liquids* (W.A. Benjamin, Inc., New York, 1966).
 - ²⁰ G.F. Giuliani and G. Vignale, *Quantum Theory of the Electron Liquid* (Cambridge University Press, Cambridge, 2005).
 - ²¹ G. Khalsa and A.H. MacDonald, *Phys. Rev. B*, **86**, 125121 (2012).
 - ²² S.E. Park and A.J. Millis, *Phys. Rev. B*, **87**, 205145 (2013).
 - ²³ G. Khalsa, B. Lee, and A.H. MacDonald, *Phys. Rev. B*, **88**, 041302 (2013).
 - ²⁴ Z.S. Popovic, S. Satpathy, and R.M. Martin, *Phys. Rev. Lett.* **101**, 256801 (2005).
 - ²⁵ P. Delugas, A. Filippetti, V. Fiorentini, D.I. Bilc, D. Fontaine, and P. Ghosez, *Phys. Rev. Lett.* **106**, 166807 (2011).
 - ²⁶ J.J. Quinn and R.A. Ferrell, *Phys. Rev.* **112**, 812 (1958).
 - ²⁷ J.B. Goodenough, *Localized to Itinerant Electronic Transitions in Perovskite Oxides* (Springer, Berlin, 1996).
 - ²⁸ S.J. Allen, B. Jalan, S. Lee, D.G. Ouellette, G. Khalsa, J. Jaroszynski, S. Stemmer, and A.H. MacDonald, *Phys. Rev. B*, **88**, 045114 (2013).
 - ²⁹ Y.J. Chang, A. Bostwick, Y.S. Kim, K. Horn, and E. Rotenberg, *Phys. Rev. B*, **81**, 235109 (2010).
 - ³⁰ P.D.C. King, S. M. Walker, A. Tamai, A. de la Torre, T. Eknapakul, P. Buaphet, S.-K. Mo, W. Meevasana, M. S. Bahramy, and F. Baumberger, *Nature Commun.* **5**, 3414 (2014).
 - ³¹ A. Joshua, S. Pecker, J. Ruhman, E. Altman, and S. Ilani, *Nature Commun.* **3**, 1129 (2012).
 - ³² C. Cancellieri, M.L. Reinle-Schmitt, M. Kobayashi, V.N. Strocov, P.R. Willmott, D. Fontaine, P. Ghosez, P. Delugas, and V. Fiorentini, *Phys. Rev. B*, **89**, 121412 (2014).
 - ³³ Although the long-wavelength low-temperature static dielectric constant of bulk SrTiO₃ is in the tens of thousands [A.S. Barker Jr. and M. Tinkham, *Phys. Rev.* **125**, 1527 (1962)] because of the presence of a soft LO phonon mode near the Γ point, the effective dielectric constant which screens electron-electron interactions is expected to be substantially smaller. The electronic transitions which contribute to the self-energy in the t_{2g} model are on the scale of a few hundred meV, much larger than the soft-phonon mode energy which is closer to a few meV [Y. Yamada and G. Shirane, *J. Phys. Soc. Jpn.* **26**, 396 (1969)]. Screening by this mode is therefore weak. Furthermore, the LO phonon mode is soft only in close vicinity to the Γ point. Even static electric fields are ineffectively screened by this mode unless they are constant over distances which greatly exceed a lattice constant. Based on these considerations, we think that the effective dielectric constant to be included in electron-electron interaction calculations is closer to $\kappa \sim 15$, similar to small-gap covalent semiconductors. All of our results are presented in terms of the parameter r_s and thus are independent of the value of κ . The conversion from r_s to density, however, does depend on κ . At liquid helium temperatures the dielectric constant of bulk SrTiO₃ is $\kappa \sim 10$ in the range 2–40 meV and $\kappa \sim 7$ above 40 meV [R.C. Neville, B. Hoeneisen and C.A. Mead, *J. Appl. Phys.* **43**, 2124 (1972)].
 - ³⁴ F.F. Fang and P.J. Stiles, *Phys. Rev.* **174**, 823 (1968).
 - ³⁵ V.M. Pudalov, M.E. Gershenson, H. Kojima, N. Butch, E.M. Dizhur, G. Brunthaler, A. Prinz, and G. Bauer, *Phys. Rev. Lett.* **88**, 196404 (2002).
 - ³⁶ Y.-W. Tan, J. Zhu, H.L. Stormer, L.N. Pfeiffer, K.W. Baldwin, and K.W. West, *Phys. Rev. Lett.* **94**, 016405 (2005).
 - ³⁷ S. Das Sarma, V.M. Galitski, and Y. Zhang, *Phys. Rev. B*, **69**, 125334 (2004).
 - ³⁸ G.D. Mahan and B.E. Sernelius, *Phys. Rev. B*, **62**, 2718 (1989).
 - ³⁹ L. Zheng and A.H. MacDonald, *Phys. Rev. B*, **49**, 5522 (1994).
 - ⁴⁰ L. Hedin, *Phys. Rev.* **139**, A79 (1965).
 - ⁴¹ A.L. Fetter and J.D. Walecka, *Quantum Theory of Many-Particle Systems* (McGraw-Hill, 1971).
 - ⁴² J. M. Luttinger, *Phys. Rev.* **119**, 1153 (1960).
 - ⁴³ D.F. DuBois, *Ann. Phys.* **8**, 24 (1959).
 - ⁴⁴ T.M. Rice, *Ann. Phys.* **31**, 100 (1965).
 - ⁴⁵ M. Kim, C. Bell, Y. Kozuka, M. Hikita, and H.Y. Hwang, *Phys. Rev. Lett.* **107**, 106801 (2011).